A NUMERICAL SIMULATION OF FLOW AND CONCENTRATION FIELDS ON MOUNTAIN LEE-SIDE

Sang Jianguo (桑建国)

Department of Geophysics, Beijing University, Beijing

and *Wu Gang* (吴 刚)

Institute of Atmospheric Physics, Academia Sinica, Beijing

Received June 26, 1985

ABSTRACT

In the present paper the numerical integration of the atmospheric thermodynamic equation system is carried out to simulate the flow and concentration fields over a two-dimensional mountain. The concentration distributions from a continuous elevated release point at different positions on the lee-side under a variety of atmospheric stabilities are calculated to examine the effects of topography on the diffusion of pollutants. The comparison between the results calculated by the model and those observed in field experiments indicates that the model can predict the transport and diffusion of pollutants under different atmospheric conditions over complex terrain and may become an applicable tool for solving the air quality problems in mountain areas.

I. INTRODUCTION

The flow and dispersion of pollutants on the lee-side of terrain obstacles are often an important part of air quality analysis in a mountain area. A number of field measurements have indicated that the stability classification given by Pasquill and Gifford (PG) as the index of turbulent diffusion rates is not necessarily valid in complex terrain. A series of tracer experiments carried out in a mountain lee-side north of Beijing shows that a shift of stable classification toward unstable appears to be appropriate for the purpose of estimating atmospheric turbulence levels. In the present paper a numerical model is used to simulate flow and concentration fields on a mountain lee-side in order to represent the phenomena described above. In particular, a form of eddy diffusivity which is able to represent turbulent diffusion processes over complex terrain is discussed. A series of experiments show that this model is suitable for predicting the distributions of pollutants on the mountain lee-side under different atmospheric conditions.

II. NUMERICAL MODEL

If the slope of terrain is not too steep, for example, less than 45°, and the terrain scale is not too small, the airflow over such terrain can be assumed to be quasi-static and impressible. Under these assumptions the motions of the air and sirborne materials can be described by the six equations (two for horizontal motion and four for hydrostatic, thermodynamic, impressible continuity and diffusion equations, respectively) with six variables u, v, w, p, θ and χ.

In order to introduce the effects of terrain the following coordinate system is used;

$$\bar{Z}=H\frac{Z-Z_g}{H-Z_g},$$

where Z is the vertical coordinate in rectangular coordinate system, Z_g the elevation of terrain, H the height of the model top. The six equations described above are transformed into a two-dimensional $(x,\bar{Z},t)$ coordinate system as follows:

$$\frac{du}{dt}=-\theta\frac{\partial\pi}{\partial x}+g\frac{\bar{Z}-H}{H}\frac{\partial Z_g}{\partial x}+K_H\frac{\partial^2 u}{\partial x^2}$$

$$+\left(\frac{H}{H-Z_g}\right)^2\frac{\partial}{\partial\bar{Z}}\left(K_m\frac{\partial u}{\partial\bar{Z}}\right)+fv, \tag{1}$$

$$\frac{dv}{dt}=fu_g+K_H\frac{\partial^2 v}{\partial x^2}+\left(\frac{H}{H-Z_g}\right)^2\frac{\partial}{\partial\bar{Z}}\left(K_m\frac{\partial v}{\partial\bar{Z}}\right)-fu, \tag{2}$$

$$\frac{d\theta}{dt}=K_H\frac{\partial^2\theta}{\partial x^2}+\left(\frac{H}{H-Z_g}\right)^2\frac{\partial}{\partial\bar{Z}}\left(K_\theta\frac{\partial\theta}{\partial\bar{Z}}\right), \tag{3}$$

$$\frac{\partial\pi}{\partial\bar{Z}}=-\frac{g}{\theta}\frac{H-Z_g}{H}, \tag{4}$$

$$\frac{\partial}{\partial x}\left(\frac{H-Z_g}{H}u\right)+\frac{\partial}{\partial\bar{Z}}\left(\frac{H-Z_g}{H}\bar{w}\right)=0, \tag{5}$$

$$\frac{d\chi}{dt}=K_H\frac{\partial^2\chi}{\partial x^2}+\left(\frac{H}{H-Z_g}\right)^2\frac{\partial}{\partial\bar{Z}}\left(K_\theta\frac{\partial\chi}{\partial\bar{Z}}\right)+S_\chi, \tag{6}$$

where χ is the concentration of airborne materials, S_χ the source strength of χ, u_g the geostrophic wind speed, π the Exner function $\pi=C_p\left(\frac{P}{P_0}\right)^{R/C_p}$ with $P_0=1000$ hPa, and the other symbols have their common meanings.

In the $(\chi,\bar{Z},t)$ coordinate system the individual derivative symbol d/dt represents

$$\frac{d}{dt}=\frac{\partial}{\partial t}+u\frac{\partial}{\partial x}+\bar{w}\frac{\partial}{\partial\bar{Z}},$$

where

$$\bar{w}=w\frac{H}{H-Z_g}+\left(\frac{\bar{Z}-H}{H-Z_g}\right)u\frac{\partial Z_g}{\partial x} \tag{7}$$

is the representation of vertical velocity in this system.

In this model we suppose the terrain to be an ideal bell-shaped mountain:

$$Z_g(x)=h\frac{a^2}{a^2+(x-x_0)^2},$$

where h and a are the height and half-width of the mountain, respectively; and x_0 the horizontal coordinate of the mountain top, and h and a are set to be 500 and 4000 m, respectively.

Altogether 90 horizontal grid-points with intervals of 500 m are taken in the model. In the vertical, the model is divided into 16 layers whose coordinates are set to be 0, 10, 30, 60, 100, 150, 200, 300, 400, 600, 800, 1000, 2000, 3000, 4000 and 5000 m, respectively.

In the integration of the prognostic Eqs. (1), (2), (3) and (6), the Chapeau function implicit

difference scheme is alternatively used in x and $\bar{Z}$ directions with time step being 10 sec (Pepper, 1979).

The boundary conditions are treated as follows:

At the bottom boundary ($\bar{Z}=0$):

$$u=v=\bar{w}=0; \quad \frac{\partial \chi}{\partial \bar{Z}}=0; \quad \frac{\partial \theta}{\partial \bar{Z}}=\text{const.}$$

At the top boundary, an absorbing layer is taken for the velocities (Klemp, 1978).

$\theta=\text{const.}, \pi=\text{const.}$, and $\frac{\partial^2 \chi}{\partial \bar{Z}^2}=0$.

At the right lateral boundary (outflow boundary), a radiative boundary condition is used for u (Orlanski, 1976). For other variables, $\frac{\partial v}{\partial x}=\frac{\partial \theta}{\partial x}=0, \frac{\partial^2 \chi}{\partial x^2}=0$.

At the left lateral boundary (inflow boundary), $u=\text{const.}$, $\theta=\text{const.}$, $\chi=0$, and $\frac{\partial v}{\partial x}=0$.

III. THE PARAMETERIZATION OF TURBULENT BOUNDARY LAYER

In the studies of advection–diffusion processes over a complex terrain by using atmospheric thermodynamic equations, it is important to seek an appropriate way to represent the turbulent processes in the planetary boundary. At present there are various forms of high-order closure schemes to solve Reynold's averaged equations. Although these representations are rather perfect theoretically, they spend much computer time and do not improve the results of simulations in any significant sense. For practical purpose the K theory is still an economic, realistic method for closing the Reynold equations. This method leads to looking for a set of appropriate parameters as the eddy diffusivities for momentum, heat and materials in the atmospheric boundary.

As air flows over an undulating terrain the spatial distributions of flow and temperature fields are deformed. Either Strengthening or weakening of vertical gradients of flow and temperature fields will alter the budget between growth and dissipation of the thermal and mechanical turbulence in the lower part of the atmosphere. At present a generally accepted representation of parameter K which can describe the turbulence processes over a complex terrain is still under discussion. The following numerical experiments will indicate that the form of the eddy diffusivities given by Businger (1971) might be a promising one.

In the surface layer which is assumed to be less than Monin–Obukhov length L, the eddy diffusivities take the forms as

$$K_i=\frac{ku_*Z}{\phi_i(Z/L)}, (Z_0 \leqslant Z \leqslant |L|) \tag{8}$$

where K_i is the eddy diffusivities for momentum ($i=m$), heat ($i=\theta$) and airborne materials ($i=\theta$); Z_0 the roughness length and L the Monin–Obukhov length.

For the neutral atmosphere, ϕ_i are taken as

$$\phi_m=1, \quad \phi_\theta=0.74.$$

For the stable atmosphere, i.e. $L>0$, we have

$$\begin{cases} \phi_m=1+4.7Z/L, \\ \phi_\theta=0.74+4.7Z/L. \end{cases} \tag{9}$$

For the unstable atmosphere, i.e. $L<0$, we have

$$\begin{cases}\phi_m=(1-15Z/L)^{-1/4},\\ \phi_\theta=(1-9Z/L)^{-1/2},\end{cases} \tag{10}$$

where L is calculated from u_* and θ_* as

$$L=\bar{\theta}\frac{u_*^2}{K_g\theta_*}, \tag{11}$$

and θ_* and u_* are given by

$$\theta_*=\kappa[\theta(Z_r)-\theta(Z_0)]/0.74[\ln(Z_r/Z_0)-\psi_\theta(Z_r/Z)], \tag{12}$$

$$u_*=\kappa u(Z_r)/[\ln(Z_r/Z_0)-\psi_m(Z_r/L)]. \tag{13}$$

Here $Z_0=0.1$ m, Z_r is the height of a grid point which is close to L, and

$$\psi_m=\begin{cases}2\ln[(1+\phi_m^{-1})/2]+\ln[(1+\phi_m^{-2})/2]-2\tan^{-1}\phi_m+\pi/2; & (L<0)\\ -4.7Z/L, & (L>0)\end{cases} \tag{14}$$

$$\psi_\theta=\begin{cases}\ln[(1+0.74\phi_\theta^{-1})/2]; & (L<0)\\ -6.35Z/L. & (L>0)\end{cases} \tag{15}$$

The values of ϕ_i, L, θ_*, u_* and ψ_i are obtained by mutual iteration. At the beginning of the integration we put a supposed value of L into (9) or (10) to obtain ϕ_m and ϕ_θ; then substitute them into (14) and (15) to get ψ_m and ψ_θ; and finally combine (12) and (13) with (11) to obtain a new value of L. The above procedure will be repeated until the relative difference of L between two successive iterations is less than 10%. At the beginning of integration four or five steps of iteration are needed. Afterwards, for every time step the iterations are generally no more than two steps. At the beginning the values of k_i vary with time considerably, then tend towards stationary as the flow and temperature fields get into a steady state. Above the surface layer the eddy diffusivities are taken as the form suggested by O'Brien (1970).

A constant value of 50 m^2 sec^{-1} is used for the horizontal eddy diffusivity K_H. In fact the magnitude of K_H has no significant sense since smoothing is taken between grid points in the processes of integration.

IV. COMPARISON BETWEEN STMULATION AND OBSERVATION

The results of the numerical simulation are compared with the observational data of the diffusion experiments carried out in a mountain area north of Beijing in 1974—1976 (Atmospheric Experiment Group, 1977a, b). Fig. 1 shows the northwest to southeast cross-section of the experimental area. In Fig. 1 A,B, and C are three release points with heights of 100, 40 and 0 m, respectively, on the lee-side. As northwest winds blew the visible smoke was released from these points. The stereophotogrammetry was used to determine the vertical and lateral diffusion deviations σ_z and σ_y.

Figs. 2—4 show the vertical diffusion deviations observed from the 18 cases classified according to different release positions and atmospheric stabilities (Atmospheric Experiment Group, 1977a). The σ_z curves observed at points A and B for stability of D and the corresponding value from flat terrain given by PG are shown in Fig. 2. From this figure it appears that, at point A on the lee-side where the flow is disturbed severely, the observed σ_z is much larger than that given by PG; and that at point B, which is still under the influence of lee-side flow fields but is further away from the mountain top than point A, the observed σ_z is three times larger than that given by PG.

The σ_z curve observed at point B in stability of C is shown in Fig. 3. It is still three times

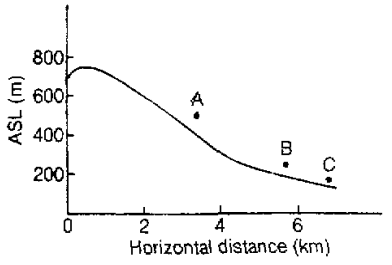

Fig. 1. Northwest-southeast cross-section of the experimental area. A.B and C indicate the positions and heights of three release points, respectively.

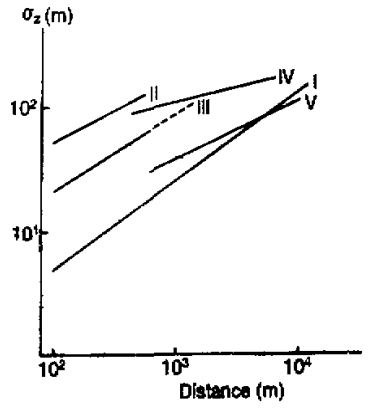

Fig. 2. σ_z-x cruves in stability of D. I—given by PG; II—observed at point A; III—observed at point B; IV—calculated on lee-side (case 1); V-calculated over flat terrain (case 2).

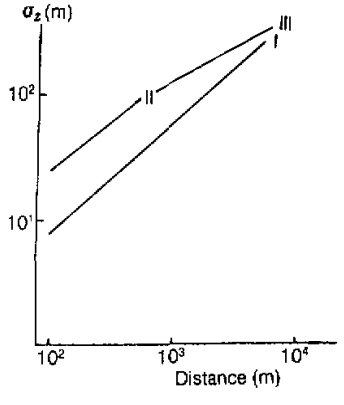

Fig. 3. σ_z-x curves in stability of C. I—given by PG; II—observed at point B; III—calculated (case 3).

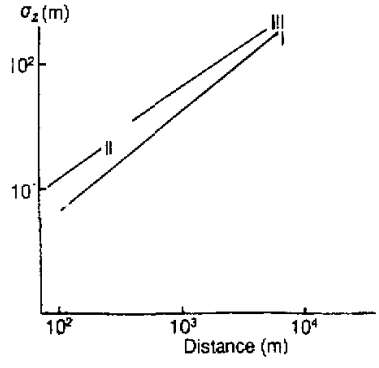

Fig. 4. σ_z-x curves in stability between C and D. I—given by PG; II—observed at point C; III—calculated (case 4).

larger than that given by PG.

Fig. 4 shows the σ_z curve observed at point C, 1 km southeast of point B. The terrain around point C is open. The smoke was released from the ground surface with the atmospheric stability ranging between C and D. The value of σ_z is twice that obtained from flat terrain. One cause for lower value of σ_z can be explained as that the release point is far from the influence of mountain lee. Another cause is that since the release is on the ground the axis of the smoke coincides with the ground surface, which keeps the smoke from vertical oscillating. This indicates that in a short distance, large-size turbulent eddies cannot play a significant role be-

cause of the constraint of the ground surface.

In order to simulate the diffusion situations on the lee-side at different release points and in different atmospheric stabilities, we design the conditions in our numerical experiments, such as the atmospheric stabilities, the positions and heights of the release points, as similar to ones in fields experiments. The results are discussed as follows.

Case 1. As similar to point A in Fig. 1, the simulated release point is located on the lee-side, 3.5 km from the mountain top, with a height of 100 m. In the two-dimensional (x, Z) section this case expresses a continuous line source with strength of 3×10^3g sec^{-1}m^{-1}. The initial wind profile is assumed as $u=1.26\ln(Z/Z_0)$, where Z_0 is 0.1 m and Z the height above the ground surface. The lapse rate Γ is set to be 0.0065 ℃ m^{-1} for the initial temperature field which can be classified into the stability of D according to NRC or MES standard (U.S. EPA, 1977; U.S. NRC, 1972). Thus the atmospheric conditions in this case are the same as those shown in Fig. 2.

As the integration time satisfies the condition of $ut/a=20$ the temperature and flow fields get into a steady stage. The distribution of the steady horizontal velocity shows that there is a region of wind maximum over the mountain top because the flow speeds up under the influence of terrain. On the lee-side another wind maximum region, about 5 km from the mountain top, can be found in the lower part of the atmosphere close to the ground surface because of the vertical momentum transport caused by wave motion. The analysis of wind velocity also indicates that strong vertical shear of the horizontal velocity exists in the first hundreds of meters on the lee-side. Fig. 5 shows the distribution of concentration simulated in this case. Because of the downslope motion of the air flow on the lee-side the axis of the smoke runs approximately parallel to the slope. This agrees with the behavior of the smoke observed in field experiments.

The curve of σ_z–x calculated according to the simulated concentration field is shown as curve IV in Fig. 2. At the first 1 km or so the calculated σ_z curve is close to curve II observed at point A, then increases at a lower rate than that of curve II. Beyond the downwind distance of 2.3 km it approaches curve III observed at point B and has a trend to approximate to curve I given by PG for flat terrain. Thus this case reflects the transient process from the strong turbulence mixing region on the lee-side to the weak turbulence region over the downwind flat plain.

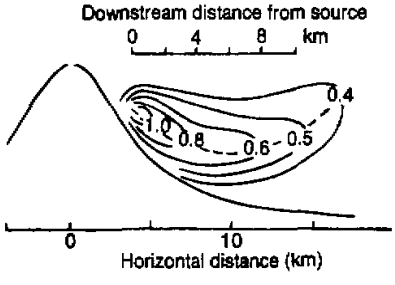

Fig. 5. Distribution of concentration calculated at t=7200 sec in case 1. Units of concentration: are g m^{-3}.

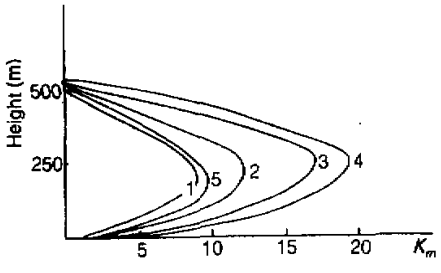

Fig. 6. K_m profiles at different positions in case 1. 1: 15 km in front of the mountain top (MT); 2: 10 km in front of the MT; 3: on the MT; 4: 4 km behind the MT; 5: 15 km behind the MT.

The intensity of the turbulence mixing in the model is expressed by the eddy diffusivities K_m and K_θ. Fig. 6 shows the K_m profiles calculated according to Eqs. (8)—(10).Gurve 1 is the profile over the flat region on the windward side far from the mountain top. As the flow arises along the windward slope K_m increases gradually (curves 2 and 3) because of intensification of the shear of the horizontal velocity and approaches the maximum on the lee-side as shown in curve 4. With the air flowing over the flat part of terrain behind the mountain, the intensity of turbulent mixing diminishes and $K_m$approaches the undisturbed situation again (curve 5).

Case 2. Using the same initial conditions of wind and temperature as in case 1, We have calculated the concentration distribution over a flat terrain, i.e. $Z(x)=0$, and obtained the value of σ_z shown as curve V in Fig. 2. Curve V is very close to curve I given by PG over the flat terrain. A comparison between cases 1 and 2 shows that this model is able to simulate the diffusion situations over different terrains and to yield the results in agreement with observations.

Case 3. In this case the initial wind condition is set to be the same as in cases 1 and 2. The initial temperature condition is as follows: The atmosphere within the first 200 m above the ground is superadiabatic with $\Gamma=0.015\ ^\circ C/m^{-1}$. Between 200 to 1000 m above the ground there is a neutral layer, and above this the atmosphere is stable with $\Gamma=0.0065\ ^\circ C/m^{-1}$. According to NRC or NES stability categories it is of C class. In this case the release point with a height of 60 m is located in the lee-side 5.5 km from the mountain top. The conditions simulated correspond to the real release situations at point B with stability of C. The comparison between the calculation and observstion is shown in Fig. 3. The value of σ_z calculated is close to that observed at point B (curve II) within short ranges and approaches curve I given by PG in flat terrain as distance increases.

Case 4. This case is assumed to simulate the release from ground-level at point C. The release point simulated has a height of 10 m, and a 10 m horizonal distance from the mountain top. The stability lies between classes C and D. The results of simulation are shown in Fig. 4.

V. SUMMARY

(1) In the present model the impact of terrain on a mountain lee-side on the flow and concentration fields is introduced and the diffusion situations from three release points at different positions of the lee-side are numerically examined. The results simulated show agreement with the observations.

(2) The form of eddy diffusivities used in the model is found to be able to reflect the turbulent mixing process in the stmospheric boundary layer over a complex terrain.

(3) This model is two dimensional. It can be expanded to become a three-dimensional one, and thus serves as a practical tool for solving the problems of air quality assessment over complex terrains.

REFERENCES

Atmospheric Experiment Group, Qinghua University and Peking University (1977a), Summary of an atmospheric experiment, Editor of Atomic Energy. (in Chinese)

Atmospheric Experiment Group (1977b), Preliminary analysis of an atmospheric experiment in mountain area, *Scientia Atmospherica Sinica*, 1: 26–35. (in Chinese with English abstract)

Businger, J.A. et al. (1971), Flux-profile relationship in the atmospheric surface layer, *J. Atmos. Sci.*, 28: 181–189.

Klemp, J.B. and Lilly, D.K. (1978), Numerical simulation of hydrostatic mountain waves, *J. Atmos. Sci.*, **32**: 78–107.

Mahrer, Y. et al. (1977), A numerical study of the air flow over irregular terrain, *Contr. to Atmos. Phys.*, **50**: 98–113.

O'Brien, J. J. (1970), A note on the vertical structure of the eddy e. change coefficient in the planetary boundary layer, *J. Atmos. Sci.*, **27**: 1213–1215.

Orlansly, I. (1976), A simple boundary condition for unbounded hyperbolic flows, *J. Comp. Phys.*, **21**: 251–269.

Pepper, C.D. et al. (1979), Modeling the dispersion of atmospheric pollution using cubic splines and Chapeau functions, *Atmos. Envir.*, **13**: 223–237.

U.S. Environmental Protection Agency (1977), Report to the U.S. EPA of the specialists conference on the EPA modeling Guidelines, February 22–24, 1977, Chicago.

U.S. Nuclear Regulatory Commission (1972), Regulatory Guide 1.23: Onsite meteorological program.